Resonance Frequency Adjustment Using PWM-Controlled Variable Capacitor for In-Motion WPT with Circuit Parameter Deviations *

Ryo Matsumoto, Bingcheng Ji, Hiroshi Fujimoto, Yoichi Hori
The University of Tokyo
5-1-5, Kashiwanoha, Kashiwa, Chiba, 277-8561 Japan
Email : matsumoto.ryo19@ae.k.u-tokyo.ac.jp

***Abstract*—In-motion wireless power transfer(WPT) is gathering attention as an effective way to provide power to electric vehicles. However, in practical use, circuit parameters deviate from nominal values due to manufacturing errors, preventing efficient and stable power transmission. The in-motion WPT system introduced in this paper actively adjusts to circuit parameter deviations using a PWM-controlled variable capacitor. This paper also proposes a variable capacitor which can be applied to in-motion WPT systems, and the validity of the proposed circuit is verified through experiment.**

***Index Terms*—wireless power transfer, resonance frequency mismatch, mistuning, variable capacitor, electric vehicle**

I. Introduction

Electric vehicles (EVs) are expected to play an important role in the sustainable development of modern society, in terms of reducing CO2 emissions. However, EVs have the drawbacks of short cruising range, long charging time and costly batteries, preventing them from becoming a popular means of transportation. In-motion wireless power transfer (WPT), an emerging technology which transmits power from the road to running electric vehicles, provides a fundamental solution to the drawbacks of EVs [1], [2]. Fig. 1 shows a typical example of a WPT circuit. The capacitors connected to the primary and secondary coils form resonant circuits. A high-frequency dc/ac inverter is connected to the primary side, and when the operating frequency of the inverter matches the resonance frequencies of the primary and secondary sides, efficient and stable power transfer is achieved [3].

However, in practical use, the values of coils and capacitors may deviate from nominal values due to manufacturing errors. This causes variations in resonance frequencies, and the desired WPT performance may not be achieved [4].

To address this problem, some improvements have been suggested in the literature [5]– [7]. Active tuning of resonance frequencies using semiconductor devices are proposed in [6], [7]. In [6], a PWM-controlled variable capacitor is proposed, which tunes the resonance frequency of the primary side. In [7], the resonance frequency of the secondary side is tuned using an active rectifier. However, neither of these researches consider resonance frequency variations on both primary and secondary sides. In addition, the variable capacitor proposed in [6] was designed for low power WPT applications such as portable devices.

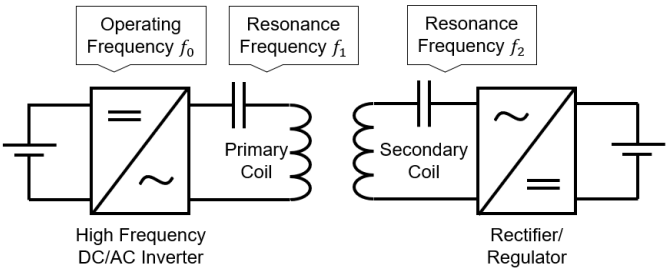

Fig. 1: Typical WPT circuit.

In this paper, a system for in-motion WPT which actively adjusts to resonance frequency variations on both primary and secondary sides is introduced. In addition, a PWM-controlled variable capacitor suited for high power WPT applications including EVs is proposed.

The remainder of this paper is organized as follows: In Section II, the in-motion WPT system capable of adjusting to resonance frequency variations is introduced. In Section III, the performance of in-motion WPT under circuit parameter deviations is evaluated. In Section IV, a variable capacitor for high power WPT applications is proposed and analyzed in comparison to the variable capacitor proposed in [6]. The validity of the proposed variable capacitor is verified through experiment in Section V, and the conclusion is drawn in Section VI.

II. In-Motion WPT System with Resonance Frequency Adjustment

Different power supply configurations for in-motion WPT have been investigated in the literature [8]– [10]. The following configuration is considered in this paper: multiple primary coils are placed in the traveling direction of the vehicle, and each coil is connected to a high frequency dc/ac inverter. A dc voltage source supplies power to each inverter.

When the resonance frequencies of coils vary due to manufacturing errors, the operating frequency of each inverter is initially fixed to the resonance frequency of the primary side. In addition, the resonance frequency of the secondary side is controlled to match the primary side by applying a variable capacitor to the secondary side.

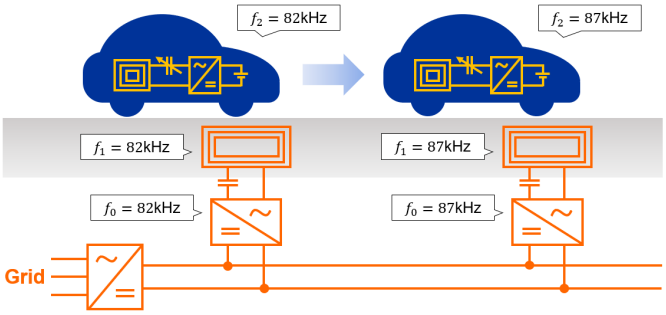

Fig. 2: Overall in-motion WPT system.

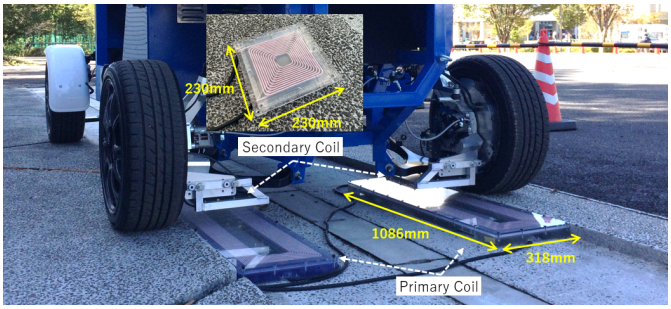

Fig. 3: Coils used for calculation and experiment.

Fig. 2 shows an example of how the system operates. The resonance frequencies of two primary coils on the WPT lane are 82 kHz and 87 kHz, respectively. The operating frequencies of the inverters connected to each coil are fixed to 82 kHz and 87 kHz. When the vehicle approaches the first coil, the resonance frequency of the secondary side is adjusted to 82 kHz, and when the vehicle moves on to the next coil the resonance frequency is adjusted to 87 kHz.

III. Performance of In-Motion WPT under Circuit Parameter Deviations

To evaluate the performance of in-motion WPT under circuit parameter deviations, the total transmission efficiency, the total energy consumed by the load and the peak current of the primary coil when a vehicle passes over a single primary coil are calculated. Three different cases including the system introduced in Section II are considered:

1) The operating frequency of the inverter is fixed to 85 kHz while resonance frequencies of the primary and secondary sides vary between 80-90 kHz.
2) The operataing frequency of the inverter is fixed to the resonance frequency of the primary side while the resonance frequencies of the primary and secondary sides vary between 80-90 kHz.
3) The operataing frequency of the inverter is fixed to the resonance frequency of the primary side while the resonance frequency of the secondary side is controlled to match the primary side (the system introduced in Section II).

The resonance frequencies are expected to vary between 80-90 kHz, assuming that the manufacturing tolerance of coils and

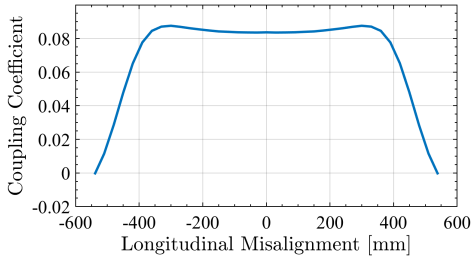

Fig. 4: Coupling coefficient between primary and secondary coils.

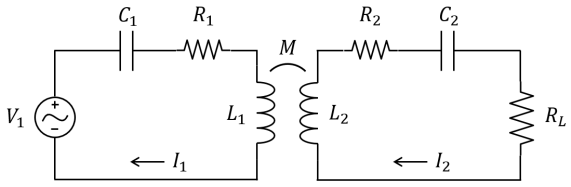

(a) Equivalent circuit model before decoupling

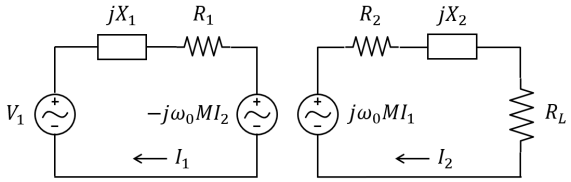

(b) Equivalent circuit model after decoupling

Fig. 5: Equivalent circuit model.

capacitors are no smaller than $\pm$ 5 %. It should be noted that this range agrees with the operating frequency range specified in the SAE J2954/1 standard [11].

The cauculation is based on the coils shown in Fig. 3. The parameters of the coils are listed in Table. I, and the coupling coefficient between the coils placed with a vertical gap of 100 mm is shown in Fig. 4. It is assumed that the secondary coil passes over the primary coil in 100 $\mathrm{km\,h^{-1}}$ with a vertical gap of 100 mm, and power transfer is activated while the coupling coefficient is higher than 0.05. The calculation is based on the equivalent circuit model shown in Fig. 5, where jX_1 and jX_2 are expressed in the following equations:

$$jX_1 = j2\pi f_0 L_1 + \frac{1}{j2\pi f_0 C_1} = j2\pi f_1 L_1 \left(\frac{f_0}{f_1} - \frac{f_1}{f_0}\right), \quad (1)$$

$$jX_2 = j2\pi f_0 L_2 + \frac{1}{j2\pi f_0 C_2} = j2\pi f_2 L_2 \left(\frac{f_0}{f_2} - \frac{f_2}{f_0}\right). \quad (2)$$

It is assumed that the RMS value of the primary voltage V_1 is fixed to 500 V, and the load resistance R_L is controlled to achieve the maximum transmission efficiency, as expressed in the following equation [12], [13]:

$$R_{Lmax} = \sqrt{R_2 \left(\frac{(\omega_0 M)^2}{R_1} + R_2\right)}. \quad (3)$$

The total transmittion efficiency and the total energy consumption is derived by the time integration of the power gen-

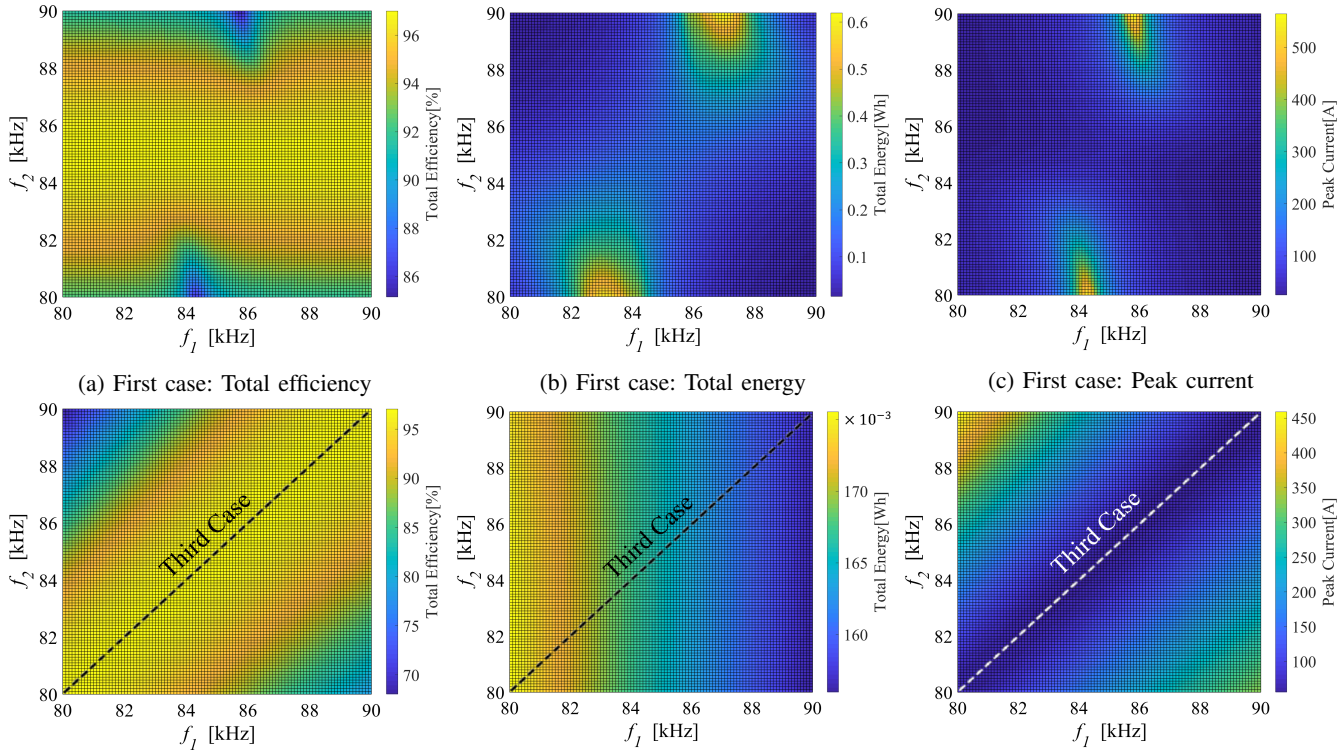

(a) First case: Total efficiency (b) First case: Total energy (c) First case: Peak current

(d) Second case: Total efficiency (e) Second case: Total energy (f) Second case: Peak current

Fig. 6: Colormaps of calculation results.

TABLE I: Coil Parameters

Symbol	Parameter	Value
L_1	Primary Coil Inductance	242 μH
R_1	Primary Coil Resistance	215 mΩ
L_2	Secondary Coil Inductance	96.0 μH
R_2	Secondary Coil Resistance	45.3 mΩ

erated by the primary voltage source and the power consumed by the load resistance. This is necessary to evaluate the performance of in-motion WPT as the transmittion efficiency and the power consumption depend on the coupling coefficient. The deviations of coil parameters originating from the alignments of the coils are neglected in the calculation.

The color maps of the calculation results are shown in Fig. 6, and the maximum and minimum values for each case are listed in Table. II. The dotted lines in Fig. 6(d)-(f) represent the calculation results for the third case.

For the first case, the total energy consumption varies between 0.02-0.62Wh. This implies that the vehicle cannot receive the desired amount of energy when there are resonance frequency variations. The maximum value of the peak current is 565A. Unexpected current peaks may lead to malfunction of the power supply system. For the second case, the total energy consumption stays within the range of 0.16-0.18Wh. However, the minimum value of the total transmittion efficiency decreases to 68.0%, and the maximum value of the peak current is 459A. For the third case, the total transmittion

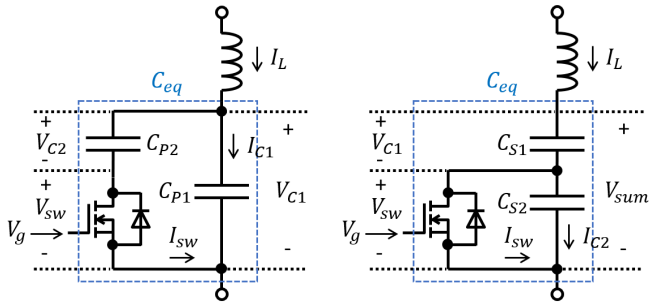

(a) Parallel type (b) Series type

Fig. 7: Circuit topology of variable capacitors.

efficiency is over 96.7%. The total energy consumption stays within the range of 0.16-0.18Wh, and the maximum value of the peak current decreases to 62.6A. By comparing the three cases, it can be concluded that the system introduced in Section II improves the efficiency and stability of in-motion WPT under circuit parameter deviations.

IV. Circuit Topology of PWM-Controlled Variable Capacitor

In previous research a PWM-controlled variable capacitor was proposed for low power WPT applications [6]. However, the following analysis verify that it is unsuitable for high power WPT applications. Fig. 7(a) shows the circuit topology

TABLE II: Representative Values of Calculation Results

	Total Efficiency(%)		Total Energy(Wh)		Peak Current(A)	
	max	min	max	min	max	min
First Case	97.0	85.1	0.62	0.02	565	24.5
Second Case	97.1	68.0	0.18	0.16	459	55.6
Third Case	97.1	96.7	0.18	0.16	62.6	55.6

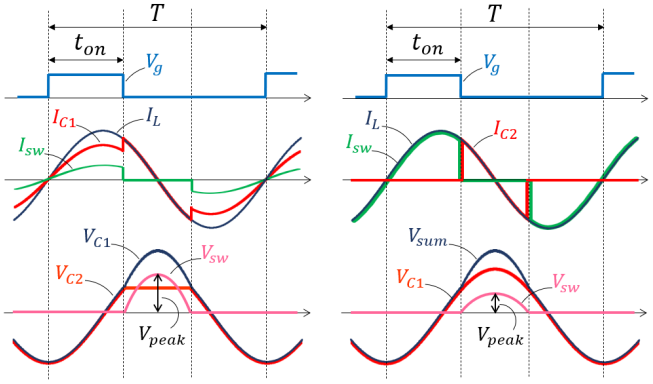

(a) Parallel type (b) Series type

Fig. 8: Waveforms of variable capacitors.

TABLE III: Variable Capacitor Parameters

Symbol	Parameter	Value
C_{P1}	Parallel Type Capacitance	32.6 nF
C_{P2}	Parallel Type Capacitance	8.70 nF
C_{S1}	Series Type Capacitance	41.3 nF
C_{S2}	Series Type Capacitance	155 nF
I_0	Current Amplitude	20 A

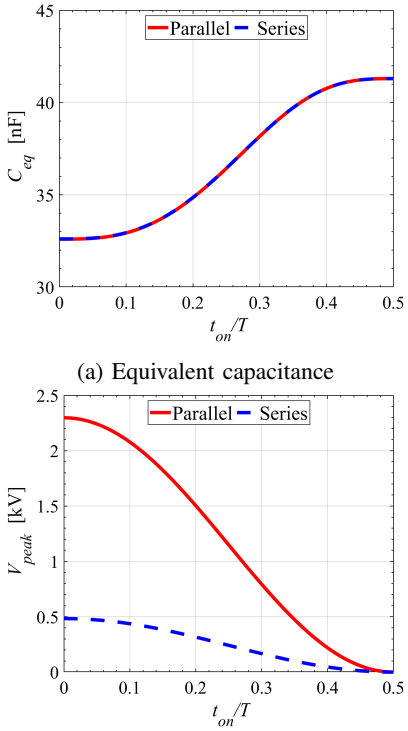

(a) Equivalent capacitance

(b) Peak voltage

Fig. 9: Comparison between parallel and series type.

of the variable capacitor proposed in [6], which is defined as the parallel type in this paper. The equivalent capacitance C_{eq} is modified by turning on the switch synchronously with the current I_L and altering the duty ratio of the PWM signal.

Fig. 8(a) shows the waveforms of the parallel type. The waveforms illustrate the capacitive characteristic of the circuit as I_L lags V_{C1} by 90 degrees. The waveform of I_L is sinusoidal, but the waveform of V_{C1} is distorted. When I_L is given by the following equation:

$$I_L = I_0 \sin\left(\tfrac{2\pi}{T}t\right), \tag{4}$$

the fundamental element of V_{C1} can be derived as the following equation:

$$V_{fund} = \tfrac{2}{T}\int_0^T V_{C1}\cos\left(\tfrac{2\pi}{T}t\right)dt = -\tfrac{TI_0}{2\pi}\left[\tfrac{1}{C_{P1}} + \left(\tfrac{1}{C_{P1}+C_{P2}} - \tfrac{1}{C_{P1}}\right)\left\{\tfrac{2t_{on}}{T} - \tfrac{1}{2\pi}\sin\left(\tfrac{4\pi t_{on}}{T}\right)\right\}\right]. \tag{5}$$

From (4) and (5), the equivalent capacitance can be derived as the following equation:

$$C_{eq} = \frac{1}{\tfrac{1}{C_{P1}} + \left(\tfrac{1}{C_{P1}+C_{P2}} - \tfrac{1}{C_{P1}}\right)\left\{\tfrac{2t_{on}}{T} - \tfrac{1}{2\pi}\sin\left(\tfrac{4\pi t_{on}}{T}\right)\right\}}. \tag{6}$$

The peak voltage between the drain and source of the switch can be derived as the following equation:

$$V_{peak} = \tfrac{1}{C_{P1}}\int_{t_{on}}^{\frac{T}{2}} I_L dt = \tfrac{TI_0}{2\pi C_{P1}}\left\{1 + \cos\left(\tfrac{2\pi t_{on}}{T}\right)\right\}. \tag{7}$$

Fig. 7(b) shows the circuit topology of the originally proposed variable capacitor, which is defined as the series type in this paper. Fig. 8(b) shows the waveforms of the series type. While the switch is turned on, the current passes through C_1 and the switch. When the switch is turned off, the current starts to pass through C_1 and C_2. When V_{sw} decreases to zero, the body diode of the switch is turned on and the current starts to pass through C_1 and the switch again.

As with the parallel type, the waveform of I_L is sinusoidal, but the waveform of V_{sum} is distorted. When I_L is given by (4), the fundamental element of V_{sum} can be derived as the following equation:

$$V_{fund} = \tfrac{2}{T}\int_0^T V_{sum}\cos\left(\tfrac{2\pi}{T}t\right)dt = -\tfrac{TI_0}{2\pi}\left[\tfrac{1}{C_{S1}} + \tfrac{1}{C_{S2}}\left\{1 + \tfrac{1}{2\pi}\sin\left(\tfrac{4\pi t_{on}}{T}\right) - \tfrac{2t_{on}}{T}\right\}\right]. \tag{8}$$

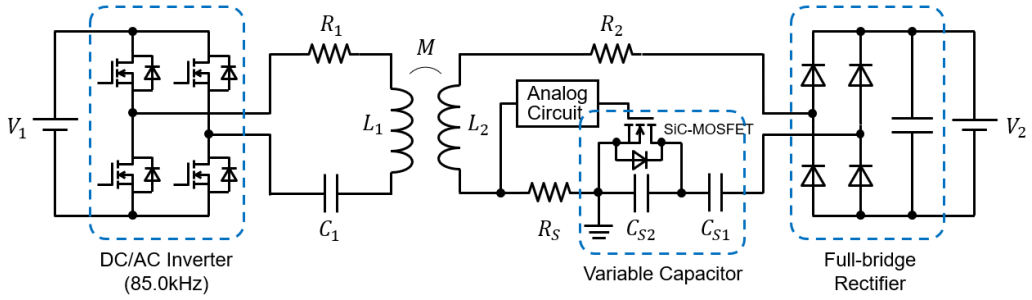

Fig. 10: WPT circuit composed for experiment.

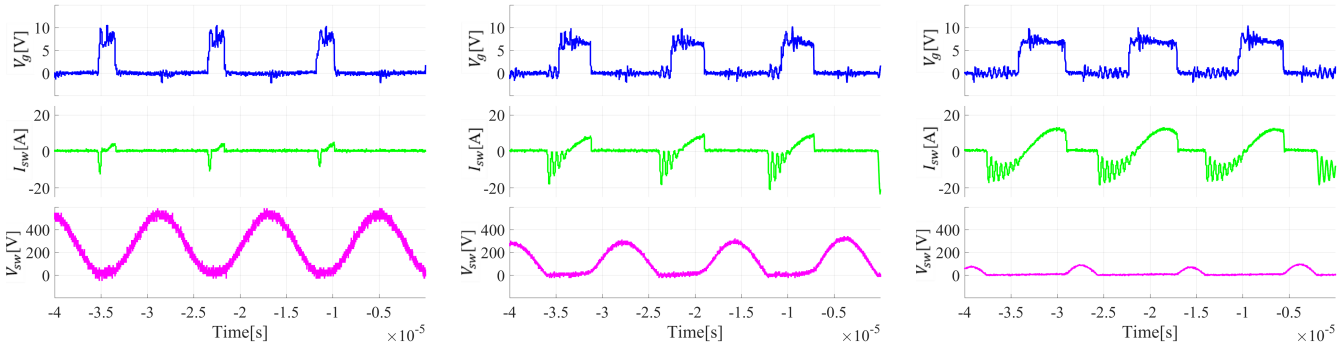

(a) $t_{on}/T = 0.08$ (b) $t_{on}/T = 0.21$ (c) $t_{on}/T = 0.36$

Fig. 11: Waveforms of the variable capacitor measured at three different duty ratios.

From (4) and (8), the equivalent capacitance can be derived as the following equation:

$$C_{eq} = \frac{1}{\frac{1}{C_{S1}} + \frac{1}{C_{S2}}\left\{1 + \frac{1}{2\pi}\sin\left(\frac{4\pi t_{on}}{T}\right) - \frac{2t_{on}}{T}\right\}}. \quad (9)$$

The peak voltage between the drain and source of the switch can be derived as the following equation:

$$V_{peak} = \frac{1}{C_{S2}}\int_{t_{on}}^{\frac{T}{2}} I_L dt = \frac{TI_0}{2\pi C_{S2}}\left\{1 + \cos\left(\frac{2\pi t_{on}}{T}\right)\right\}. \quad (10)$$

In the following analysis the performance of the parallel and series type are compared when they are applied to the secondary side of the WPT circuit. The analysis is based on the secondary coil inductance listed in Table. I, and the resonance frequency of the secondary side is assumed to be controllable between 80-90kHz. From these assumptions, the available range of the equivalent capacitance should be 32.6-41.3nF, and the parameters listed in Table. III are selected to satisfy this range. Fig. 9 is obtained by substituting the parameters in Table. III to (6), (7) and (9), (10). From Fig. 9(a) the equivalent capacitance of both types change continuously between 35.3-44.6nF depending on the duty ratio. From Fig. 9(b) the peak voltage of the parallel type can be higher than 2 kV, while the peak voltage of the series type is constantly lower than 0.5 kV. This indicates that the series type is more suitable for high power WPT applications as the breakdown voltage of SiC-MOSFETs are usually lower than 1 kV.

TABLE IV: Experiment Parameters

Symbol	Parameter	Value
V_1	Primary DC Voltage	50 V
V_2	Secondary DC Voltage	50 V
L_1	Primary Coil Inductance	242 µH
R_1	Primary Coil Resistance	215 mΩ
L_2	Secondary Coil Inductance	96.0 µH
R_2	Secondary Coil Resistance	45.3 mΩ
C_1	Primary Compensation Capacitance	14.4 nF
C_{S1}	Secondary Compensation Capacitance	41.3 nF
C_{S2}	Secondary Compensation Capacitance	114 nF
M	Mutual Inductance	10.6 µH
R_S	Shunt Resistance	200 mΩ

V. Experiment

The circuit shown in Fig. 10 is composed to verify the performance of the series type variable capacitor. The parameters of the circuit are listed in Table. IV. The primary and secondary coils shown in Fig. 3 are placed with a vertical gap of 100 mm, and the secondary coil is connected to the series type variable capacitor. The analog circuit is composed to generate PWM signals synchronized with the secondary side current. The operating frequency of the inverter is fixed to 85.0 kHz. According to the parameters listed in Table. IV, the resonance frequency of the primary side is 85.2 kHz, and the resonance frequency of the secondary side is controllable between 79.9-93.3 kHz. The transmittion efficiency, the power consumed by the load and the waveforms of the variable capacitor are measured while the duty ratio of the PWM signal

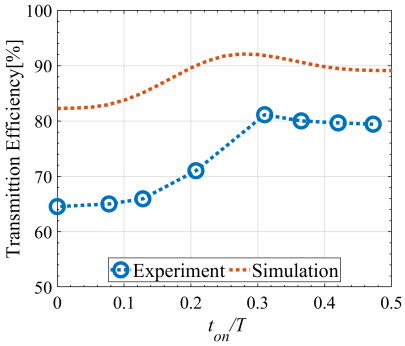

(a) Transmittion efficiency

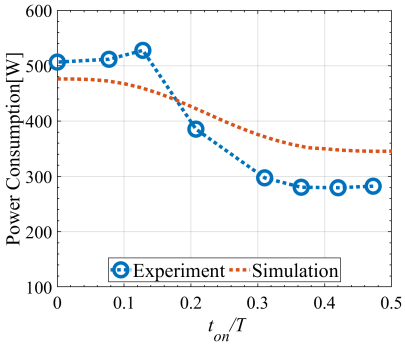

(b) Power consumption

Fig. 12: Experiment results of transmission efficiency and power consumption.

is altered between 0-0.5.

Fig. 11 shows the waveforms of the gate signal V_g, the switch current I_{sw} and the switch voltage V_{sw} measured at three different duty ratios. The series type variable capacitor is functioning appropriately as the measured waveforms shown in Fig. 11(c) roughly correspond to the theoretical waveforms shown in Fig. 8(b). Moreover, V_{sw} does not exceed the breakdown voltage of the SiC-MOSFET as the peak value of V_{sw} is lower than 600 V. It is assumed that the damped oscillations visible in the waveforms of I_{sw} result from parasitic inductances in the circuit of the variable capacitor.

Fig. 12 shows the experiment results of the transmittion efficiency and the power consumption along with the simulation results. The simulation is implemented with the same circuit shown in Fig. 10, except the variable capacitor is replaced by an ordinary capacitor. The value of the capacitor is determined by (9). The experiment results and the simulation results show similar features. This indicates that the series type variable capacitor is capable of adjusting the resonance frequency of the secondary side. The experiment result of the transmittion efficiency is more than 10 points lower than the simulation result. The major cause of this difference is assumed to be the conduction loss and switching loss of the SiC-MOSFET. Another explanation for the difference between the experiment results and the simulation results is the measurement errors of the parameters listed in Table. IV.

VI. Conclusion

In this paper, a system for in-motion WPT which actively adjusts to resonance frequency variations using a PWM-controlled variable capacitor was introduced. The evaluation of in-motion WPT performance verified that this system provides efficient and stable power transmittion under circuit parameter deviations. Also, a PWM-controlled variable capacitor which can be applied to high power WPT applications was proposed. The function of this variable capacitor was confirmed by experiment. The experiment also verified that this variable capacitor is capable of adjusting the resonance frequency of the secondary side. Future work includes the experimental verification of the overall in-motion WPT system introduced in this paper.

Acknowledgment

This work was partly supported by JSPS KAKENHI Grant Number 19H02123 and JST-Mirai Program Grant Number JPMJMI17EM, Japan.

References

[1] O. C. Onar, J. M. Miller, S. L. Campbell, C. Coomer, C. P. White and L. E. Seiber, "A Novel Wireless Power Transfer for In-Motion EV/PHEV Charging," IEEE Applied Power Electronics Conference and Exposition (APEC), pp.3073-3079, 2013.

[2] O. Shimizu, S. Nagai, T. Fujita and H. Fujimoto, "Potential for CO2 Reduction by Dynamic Wireless Power Transfer for Passenger Vehicles in Japan," Energies 2020, 13, 3342.

[3] G. A. Covic and J. T. Boys, "Inductive Power Transfer," Proc. IEEE, vol. 101, no. 6, pp. 1276-1289, 2013.

[4] H. Weerasekara, K. Hata, T. Imura, H. Fujimoto and Y. Hori, "Efficiency Maximization in Wireless Power Transfer Systems for Resonance Frequency Mismatch," 2019 IEEE PELS Workshop on Emerging Technologies: Wireless Power Transfer, 2019.

[5] W. Li, H. Zhao, J. Deng, S. Li and C. C. Mi, "Comparison Study on SS and Double-Sided LCC Compensation Topologies for EV/PHEV Wireless Chargers," IEEE Transactions on Vehicular Technology, vol. 65, no. 6, pp. 4429-4439, 2016.

[6] D. Kim and D. Ahn, "Self-Tuning LCC Inverter Using PWM-Controlled Switched Capacitor for Inductive Wireless Power Transfer," IEEE Transactions on Industrial Electronics, vol. 66, no. 5, pp. 3983-3992, 2019.

[7] R. Mai, Y. Liu, Y. Li, P. Yue, G. Cao and Z. He, "An Active-Rectifier-Based Maximum Efficiency Tracking Method Using an Additional Measurement Coil for Wireless Power Transfer," IEEE Transactions on Power Electronics, vol. 33, no. 1, pp. 716-728, 2018.

[8] J. Huh, S. W. Lee, W. Y. Lee, G. H. Cho and C. T. Rim, "Narrow-Width Inductive Power Transfer System for Online Electrical Vehicles," IEEE Transactions on Power Electronics, vol. 26, no. 12, 2011.

[9] L. Chen, G. R. Nagendra, J. T. Boys and G. A. Covic, "Double-Coupled Systems for IPT Roadway Applications," IEEE Journal of Emerging and Selected Topics in Power Electronics, vol. 3, no. 1, 2015.

[10] A. N. Azad, A. Echols, V. A. Kulyukin, R. Zane and Z. Pantic, "Analysis, Optimization, and Demonstration of a Vehicular Detection System Intended for Dynamic Wireless Charging Applications," IEEE Transactions on Transportation Electrification, vol. 5, no. 1, pp. 147-161, 2019.

[11] Wireless Power Transfer for Light-Duty Plug-In/Electric Vehicles and Alignment Methodology, Standard SAEJ2954, 2016.

[12] D. Kobayashi, T. Imura and Y. Hori, "Real-time Coupling Coefficient Estimation and Maximum Efficiency Control on Dynamic Wireless Power Transfer for Electric Vehicles," 2015 IEEE PELS Workshop on Emerging Technologies: Wireless Power, 2015.

[13] B. Ji, K. Hata, T. Imura, Y. Hori, S. Shimada and O. Kawasaki, "Wireless Power Transfer System Design with Power Management Strategy Control for Lunar Rover," IEEJ Journal of Industry Applications, vol. 9, no. 4, pp. 392-400, 2020.